Dalton Transactions

ROYAL SOCIETY OF CHEMISTRY

PAPER

View Article Online
View Journal | View Issue

Cite this: *Dalton Trans.*, 2025, **54**, 12859

On the structure of heptalithium distannide: Li_7Sn_2 or $Li_{7-x}Sn_2$ ($0.3 < x < 0.5$)

Salina Rahman, [a] Kowsik Ghosh, [a] Alexander Ovchinnikov, [a,b] Anirudh Nandakumar, [c] Candace K. Chan [c] and Svilen Bobev *[a]

Received 30th April 2025,
Accepted 22nd July 2025

DOI: 10.1039/d5dt01022e

rsc.li/dalton

Li–Sn intermetallics are promising candidates for high-capacity Li-ion battery anodes, yet, the precise crystal structures of some "known" binary phases remain unresolved. One such phase, Li_7Sn_2, originally reported in 1975, is re-examined here using single-crystal X-ray diffraction methods. Its orthorhombic structure (space group *Cmmm*, no. 65) features isolated Sn atoms and Sn–Sn dumbbells in a matrix of Li atoms. The present study indicates occupational disorder on one of the Li sites in Li_7Sn_2, meaning that it is a non-stoichiometric phase with revised composition of $Li_{7-x}Sn_2$ ($0.3 < x < 0.5$). In the most extreme case, when the Li atomic site in question is completely empty, the composition becomes $Li_{6.5}Sn_2$ or $Li_{13}Sn_4$. Analysis of the chemical bonding through electronic structure calculations indicates significant covalency of Sn–Sn and Li–Sn interactions.

Introduction

Lithium-ion batteries (LIBs) are rechargeable energy storage devices that have become widely used since their introduction in the early 1990s. Graphite is the typical anode in LIBs, as it has a good cycling performance with a theoretical capacity of 372 mAh g^{-1} (LiC_6).[1] The other group 14 elements, referred to as tetrels, Si, Ge, and Sn, have also been studied for application as potential anode materials in LIBs. The tetrels (Tt = Si, Ge, and Sn, hereafter) form a variety of intermetallic Li_xTt_y compounds with Li, some of which are rather Li-rich. Hence, compared to graphite, Si, Ge, and Sn can provide much higher theoretical capacities: 4200 mAh g^{-1} for $Li_{17}Si_4$, 1600 mAh g^{-1} for $Li_{17}Ge_4$, and 990 mAh g^{-1} $Li_{17}Sn_4$.[1]

However, the volume expansion in fully lithiated states is problematic (*viz.* 434% (399%) for amorphous (crystalline) Li–Si[2]), leading to diminished capacity and reduced lifespan. Although not as attractive from the point of view of increased weight, Li–Ge/Sn compounds are gaining attention as more viable alternatives for LIB applications since their volume expansions are significantly smaller, especially for Sn.[2] To design and develop improved anode materials, one can argue that it is essential to gain a deeper understanding of the structural chemistry of the various Li–Ge and Li–Sn phases that form during the lithiation of Ge- and Sn-based anodes.

The early structural work on the binary Li–Sn phases is from the 1950s/1960s. Based on literature searches and the information found in the ICSD (Inorganic Crystal Structure Database), there are eight crystallographically characterized Li–Sn phases and these are: Li_2Sn_5 [3] (the correct composition and structure of a phase initially reported as $LiSn_2$ [3]) LiSn,[4] Li_7Sn_3,[5] Li_5Sn_2 (or rather $Li_{5-x}Sn_{2+x}$),[6,7] $Li_{13}Sn_5$,[8] Li_7Sn_2,[9] $Li_{17}Sn_4$ (or $Li_{17.05}Sn_4$, previously known as $Li_{21}Sn_5$ and/or $Li_{22}Sn_5$ and often referred to as $Li_{4.4}Sn$),[10,11] and Li_5Sn, which has the highest amount of Li.[12] The latter is also the most recently discovered phase, which is metastable and not found in the experimental phase diagram.[13] Theoretical predictions indicate the presence of additional, hitherto unidentified members near the bottom of the convex hull. For example, high-throughput density functional theory (DFT) calculations on the Li–Sn systems indicate several ground-state and metastable crystal structures, such as Li_2Sn_3, Li_2Sn, Li_3Sn_2, Li_5Sn_3, Li_8Sn_3, Li_3Sn, Li_4Sn, and Li_7Sn,[14] none of which have been experimentally confirmed to date.

In addition to the structures of the two thermodynamically stable phases that have already been re-assessed, there remain controversies surrounding the Li_7Sn_2 phase. The latter was discovered in 1975 and reported to be isotypic with Li_7Ge_2 (published in 1972[15]). However, in 1988, the composition of the Li_7Ge_2 phase has been questioned,[16] and suggested to be $Li_{6.5}Ge_2 \equiv Li_{13}Ge_4$. The proposed reformulation of Li_7Ge_2 as $Li_{13}Ge_4$ [16] precedes by more than two decades the re-examination of the structure of $Li_{13}Si_4$, which had also been previously known as Li_7Si_2 (N. B. $Li_{13}Si_4$ and $Li_{13}Ge_4$ are not iso-

[a]*Department of Chemistry and Biochemistry, University of Delaware, Newark, Delaware 19716, USA. E-mail: bobev@udel.edu*
[b]*Faculty of Chemistry and Food Chemistry, Technische Universität Dresden, 01062 Dresden, Germany*
[c]*Materials Science and Engineering, School for Engineering of Matter, Transport and Energy, Arizona State University, P.O. Box 876106, Tempe, Arizona 85827, USA*

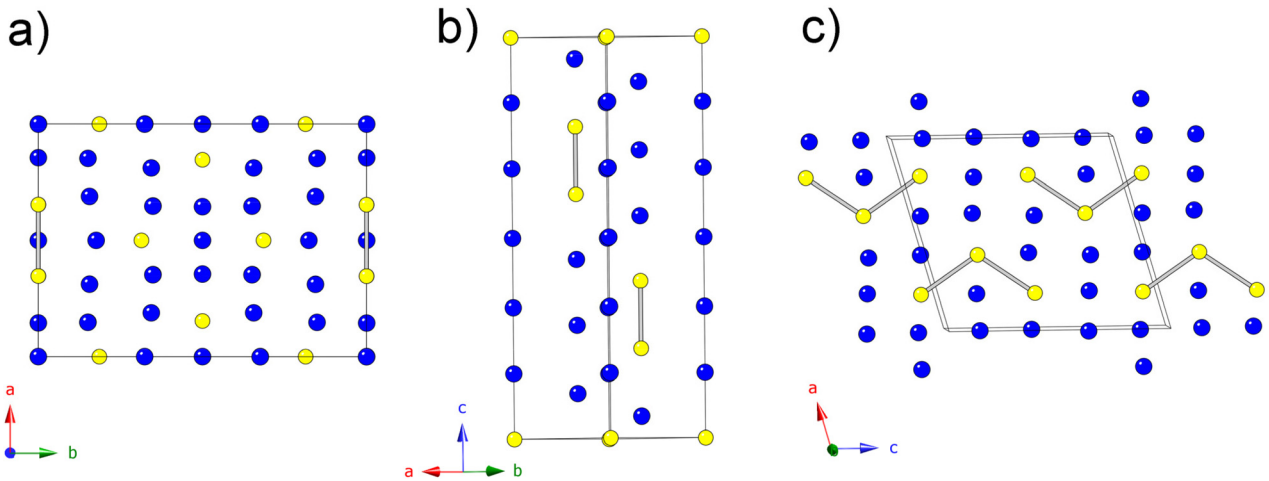

Fig. 1 Schematic representations of the crystal structures of (a) Li_7Sn_2, (b) $Li_{13}Sn_5$, and (c) Li_7Sn_3. Blue represents Li atoms, Sn atoms are drawn in yellow.

structural).[17] In the case of the Li–Si system, very careful refinement of the structure from single-crystal X-ray diffraction data carried out by Fässler *et al.* identified discrepancies with regards to the occupation of Li on one of the positions,[18] which validates a revised model. It is acknowledged though, right at the outset, that because lithium may show high mobility within the structure and it has only three electrons (compared to germanium's 32 and tin's 51), achieving a more accurate description of lithium positions and occupancies in Li–Ge/Sn compounds may be more challenging.

Having said that, we note that in our previous work,[7] the crystal structures of Li_5Sn_2 and Li_5Ge_2 were re-examined, highlighting the structural intricacies among the heavier carbon congeners. Specifically, it was established that the Li and Sn atoms in $Li_{5-x}Sn_{2+x}$ ($0 < x < 0.1$) exhibit partial disorder.[7] This partial substitution of lithium by tin atoms leads to more complex atomic bonding, with the Sn atoms forming larger covalently bonded fragments. In contrast, both experimental and computational evidence indicated that in the structure of the phase hitherto known as Li_5Ge_2, there are approximately 30% vacancies at one of the lithium sites, with the actual chemical formula being $Li_{5-x}Ge_2$ ($x \approx 0.3$). The latter composition is very close to that of the "Li_7Ge_3" phase, which has only been theoretically predicted.[19] One should be aware that the work computing Li_7Ge_3 was carried out using the atom swapping method by combining the *ab initio* random structure searching procedure (AIRSS) to perform structure prediction from density functional theory (DFT).[19] Our experimental work[7] cannot quite validate the computationally suggested structure, but it does show that in rhombohedral $Li_{5-x}Ge_2$ ($x \approx 0.3$), the [Ge_2] dimers are slightly more "oxidized" and show bond order intermediate between 1 and 2.

The above-mentioned studies raise questions of potential undetected disorders in other compositionally/structurally similar Li–Ge/Sn phases. Therefore we set out to revisit some of the other structures with smaller, molecular-like fragments, *e.g.* [Tt_2] dimers and [Tt_3] trimers (Fig. 1). In particular, our interest was piqued by the reported Li_7Tt_2 (Tt = Ge, Sn) phases, which are the Li-richest phases whose structures feature homoatomic Tt–Tt bonding; we found the structure of both heptalithium germanide and stannide to be Li-deficient, *i.e.*, $Li_{7-x}Tt_2$. As part of our investigation, using modern single-crystal X-ray diffraction methods, we also re-examined the crystal structures of Li_7Sn_3, and $Li_{13}Sn_5$, which are unique to the Li–Sn phases and have no structural analogs among the known Li–Ge phases; we found both structures to be devoid of any disorder.

Experimental

Synthetic procedures

Handling of the raw and synthesized materials required the use of a glovebox filled with argon gas (maintaining O_2/H_2O levels below one ppm) and vacuum techniques. This was done in order to protect the air-sensitive reactants and products. Samples were prepared using the traditional solid-state method in sealed tubes. Li and Sn (or Ge) were the starting materials, which were sourced from Sigma–Aldrich and Alfa Aesar with purities of at least 99.9% by weight. Lithium rods were cleaned with a scalpel immediately before being used to remove surface impurities from Li_3N. The elements were weighed with molar ratios varying from *ca.* 4 : 1 to 2 : 1. Some of the findings from these experiments have already been reported.[7] In this article we focus on the nominal compositions Li : Sn = 7.5 : 2, 7.0 : 2, 6.7 : 2, 6.5 : 2, 6.25 : 2, and 6.0 : 2. In the typical experiments, 300–400 mg elemental mixtures were placed into niobium tubes, which were then welded shut under partial pressure of high purity argon gas. Then, the niobium tubes were enclosed in fused silica tubes, which were evacuated and flame sealed.

The processing was done in programmable tube furnaces, which were brought to 1123 K at a rate of 100 K per hour. The reactions took place over two hours, following which the furnaces were set to controlled cooling at a rate of 25 K per hour. Once at room temperature, the reaction vessels were removed from the furnaces; the fused silica tubes were cut and the welded tubes were returned to the glovebox and carefully opened to retrieve the final products.

Caution! Lithium vapors can leak from the niobium tubes at high temperature and cause the breakage of the fused silica jackets. Therefore, all described experimental procedures have to be performed with utmost care and by using additional precautions to minimize the risk of failure of the silica tubes.

Crystallography

Powder X-ray diffraction. Powder X-ray diffraction (PXRD) experiments were conducted at room temperature on freshly prepared polycrystalline samples. Small portions from each reaction's products were ground in the glovebox into powders, using agate mortars and pestles. The samples were loaded into thin-walled capillary tubes (0.5 mm diameter special glass capillary tubes from Charles Supper). Samples were prepared in the Ar glovebox and the capillary ends were sealed with clay. Then the capillaries were placed in a plastic tube, which was closed and sealed with parafilm, then heat sealed inside a polybag for transport to the diffractometer to minimize air exposure until the measurement (N. B. the measurement was done at ambient conditions). A STOE STADI P diffractometer with monochromatized Ag Kα radiation (λ = 0.55941 Å) with four single module strip detectors (Mythen2 1K Dectris) was utilized and data were collected up to 73.335° in 2θ with a step size of 0.015° for a total scan-time of 30 minutes.

Single-crystal X-ray diffraction. Single-crystal X-ray diffraction (SCXRD) data were gathered for crystals from samples of different nominal compositions. Abbreviated crystallographic parameters for two $Li_{7-x}Sn_2$ crystals selected from samples with nominal compositions Li : Sn = 7.0 : 2 (crystal **A**), and 6.0 : 2 (crystal **B**) are tabulated in Table 1; the corresponding data for three additional $Li_{7-x}Sn_2$ crystals are available as SI (Table S1). Also in the SI section, one can find complementary structure refinements for three $Li_{7-x}Ge_2$ crystals (Table S2). To ascertain the presented crystallographic work, additional analyses were also performed for Li_7Sn_3 (from two independent samples), $Li_{13}Sn_5$ (from two independent samples), and $Li_{17}Sn_4$ crystals, with the data available in Tables S3–S5.

The general procedure was the following. First, single crystals were selected in an argon-filled glovebox under a microscope. They were emersed in a droplet of dry Paratone-N oil and cut with a scalpel, ensuring their dimensions were ≤0.2 mm. The samples were them taken out of the glovebox and the selected crystals were scooped from the oil drop by MiTeGen plastic loops and transferred to a Bruker APEX III diffractometer with monochromatized Mo Kα radiation (λ = 0.71073 Å). Data collection was performed at a temperature of 200(2) K, which was maintained using a stream of cold nitrogen gas. Raw data sets were processed using the Bruker software and corrected for absorption with the SADABS software package. Crystal structures were solved by the intrinsic phasing method using SHELXT and refined by full-matrix least-squares methods on F^2 with SHELXL, with the OLEX2 program as graphical interface.[20–22] Atomic coordinates were standardized with Structure TIDY.[23] Sn (and Ge) atoms were refined with anisotropic displacement parameters, while the Li atoms in $Li_{7-x}Tt_2$ were treated isotropically without further constraints. For the structure refinements of Li_7Sn_3 and $Li_{13}Sn_5$, both of which are free of any disorder, all or nearly all atoms could be refined with anisotropic displacement parameters. For the structure refinements of $Li_{17}Sn_4$ (Table S5), one of the 13 Li sites had to have its U_{iso} constrained (*vide infra*).

The Cambridge Crystallographic Data Centre (CCDC) contains the full supplementary crystallographic data. The respective CIFs have depository numbers 2444618–2444627, 2444630, 2444633 and 2444635.

Table 1 Crystallographic information for two representative $Li_{7-x}Sn_2$ (0.3 < x < 0.5) crystals. T = 200(2) K; Mo Kα, λ = 0.71073 Å; crystal system: orthorhombic, space group: *Cmmm*, Z = 4

	Crystal **A**	Crystal **B**
Refined chemical formula	$Li_{6.67(3)}Sn_2$	$Li_{6.5}Sn_2$
Formula weight (g mol^{-1})	283.69	282.49
a (Å)	9.7882(13)	9.8176(13)
b (Å)	13.842(2)	13.826(2)
c (Å)	4.7333(6)	4.7187(6)
V (Å^3)	641.29(15)	640.52(15)
ρ_{calc} (g cm^{-3})	2.94	2.93
μ (cm^{-1})	76.3	76.4
Goodness-of-fit on F^2	1.083	1.056
R_1 ($I \geq 2\sigma_I$)[a]	0.0220	0.0359
wR_2 ($I \geq 2\sigma_I$)[a]	0.0395	0.0580
R_1 (all data)[a]	0.0275	0.0558
wR_2 (all data)[a]	0.0408	0.0627
$\Delta\rho_{max,min}$/e$^-$ Å^{-3}	1.13/−1.00	1.56/−1.51
CCDC number	2444619	2444622

[a] $R_1 = \sum||F_o| - |F_c||/\sum|F_o|$; w$R_2 = [\sum[w(F_o^2 - F_c^2)^2]/\sum[w(F_o^2)^2]]^{1/2}$, where $w = 1/[\sigma^2F_o^2 + (xP)^2 + (yP)]$, and $P = (F_o^2 + 2F_c^2)/3$. x = 0.0126, y = 0.4756 for $Li_{6.67(3)}Sn_2$; x = 0.0229, y = 0.2352 for $Li_{6.5}Sn_2$.

Electronic structure calculations

The electronic band structures were computed using the Stuttgart TB-LMTO-ASA code, applying the local density approximation (LDA) for the exchange–correlation functional.[24] Specifically, the von Barth–Hedin version of the LDA functional was used.[25] Additional empty spheres were introduced where necessary to fulfil the atomic sphere approximation (ASA) requirements. The Brillouin zone was sampled with a k-point grid of 6 × 6 × 10. Chemical bonding analysis was carried out using the Crystal Orbital Hamilton Population (COHP) method.[26]

Total energy calculations were carried out using the Quantum ESPRESSO 7.4 program package[27] for Li_7Sn_2, $Li_{13}Sn_5$, as well as two $Li_{7-x}Sn_2$ models: $Li_{13}Sn_4$ (x = 0.5) and $Li_{27}Sn_8$ (x = 0.25). Exchange and correlation were described in

the generalized gradient approximation (GGA) with the Perdew–Burke–Ernzerhof exchange–correlation functional (PBE).[28] A plane wave basis with a kinetic energy cutoff of 70 Ry and ultrasoft Vanderbilt pseudopotentials were employed.[29] The Brillouin zones were sampled with a *k*-point grid spacing of about 0.15 Å^{-1}. The starting structure of $Li_{6.5}Sn_2 \equiv Li_{13}Sn_4$ was taken from directly from the single-crystal refinements, where the 2*a* Li site was found to be completely empty (*vide infra*). The $Li_{27}Sn_8$ model was generated from the structure of $Li_{13}Sn_4$ by reducing the space group symmetry down to *Pmmm* without changing the conventional unit cell size and placing a Li atom in 1*d* or 1*g* position (both options result in symmetry equivalent structures). All structures were fully relaxed to residual forces of less than 0.01 eV Å^{-1}.

Results and discussion

Synthesis and crystal structure

As indicated in the previous section, several $Li_{7-x}Sn_2$ nominal compositions were tried and the corresponding PXRD patterns are shown in Fig. 2. A close look at the PXRD patterns for the nominal compositions Li_7Sn_2 and $Li_{6.7}Sn_2$ shows that they match very well with the simulated pattern, with only faint additional peaks originating from a minor secondary phase. As the lithium content decreases to the nominal composition $Li_{6.5}Sn_2$, stronger additional peaks (black asterisk) that do not match the reference Li_7Sn_2 pattern emerge. Upon further reduction in lithium content to nominal composition of 6.25 : 2, the PXRD pattern still shows peaks consistent with Li_7Sn_2; however, more intense peaks corresponding to the additional phase, identified as $Li_{13}Sn_5$ become more evident. Finally, the sample with nominal composition Li_6Sn_2 exhibits distinct diffraction peaks associated with a different phase, $Li_{13}Sn_5$, together with peaks matching the Li_7Sn_2 phase. The peaks' relative intensities here are suggestive of Li_7Sn_2 being the minor product. These findings are in a reasonably good agreement with the established Li–Sn phase diagram,[13] which indicates Li_7Sn_2 and $Li_{13}Sn_5$ to be in equilibrium around 75 at% Li.

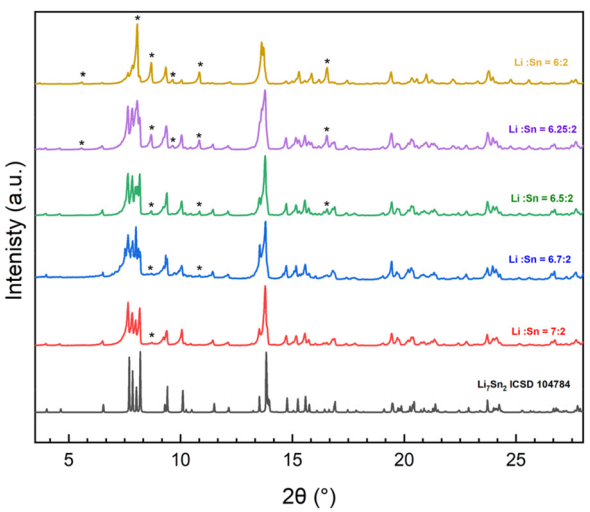

Fig. 2 Experimental powder X-ray diffraction (PXRD) patterns of samples with varying nominal compositions (Li : Sn = 7 : 2, 6.7 : 2, 6.5 : 2, 6.25 : 2, and 6 : 2) compared with the simulated PXRD pattern based on the reported data for Li_7Sn_2.[9] Asterisks denote peaks from side products, which in the cases of Li : Sn = 6.25 : 2, and Li : Sn = 6 : 2 have been determined to be $Li_{13}Sn_5$. Data are acquired with monochromatized Ag Kα radiation (λ = 0.55941 Å).

Additionally, we note that upon increasing of lithium content (samples with nominal compositions of 7.25 : 2 and 7.50 : 2), the pathway to $Li_{7-x}Sn_2$ appears to shut off. Such experiments predominantly yielded the cubic $Li_{17}Sn_4$ phase,[10] with indications of another, yet unidentified phase. This may suggest more complex phase relationships than the equilibria near 80 at% Li that are indicated in the phase diagram.[13]

The PXRD patterns show no systematic changes in the lattice parameters that could point to sample dependence on the experimental conditions, which helps to rule out significant stoichiometry range in $Li_{7-x}Sn_2$. This scenario is distinctly different from what was observed for the phase $Li_{5-x}Sn_{2+x}$ ($0 < x < 0.1$), whose structure was recently revisited from Li_5Sn_2 and found to be partially disordered.[7] Nonetheless, from single-crystal X-ray diffraction data, small variations in the lattice parameters were found, even for crystals selected from the same batch. This observation is indicative of small disordering, possibly resulting from partial occupation of Li site(s). By comparison, contrasting behavior can be seen for the other phase that was a common by-product of our syntheses, $Li_{13}Sn_5$—when we examined crystals from two independent preparations, no statistically significant deviations in the lattice parameters were found (Table S3 in SI).

To gain better understanding of the potential structural changes that can be inferred from the discussion above, single-crystal X-ray diffraction analysis was conducted for five crystals from independent $Li_{7-x}Sn_2$ reaction batches. The results from the structure refinements confirmed that none of the collected data sets can be matched properly to the reported Li_7Sn_2 structure.[9] Specifically, one of the lithium sites in the published "7–2" structure, the special 2*a* Wyckoff position (Table 2, Fig. 3), was found to be empty, or rather, not entirely filled by Li. Acknowledging the inaccuracy of refining Li occupancy factors from X-ray diffraction, we draw attention to the fact that in all refined structures, the difference Fourier maps are flat with highest residual density of less than 1.3 e Å^{-3}. In only one case, namely, the crystal from the nominal composition 7 : 2, a small residual peak was located at coordinates 0,0,0. When refined as partially occupied Li, the corresponding site occupation factor was approximately 35%. If this position is assigned as Li6 at full occupancy, its U_{iso} parameter becomes 20 times larger than the average U_{iso} of the other Li atoms in the structure. One may also notice that Li6 has four Li2 neighbors at a distance of approx. 2.5 (2.3 Å in $Li_{7-x}Ge_2$, the structure of which was also refined as a part of this study – Tables S2 and S7 in SI) which is very short for a Li–Li contact. At the same time, refining Li2 occupancy does not provide

Table 2 Atomic coordinates and equivalent isotropic displacement parameters (U_{eq} [a] in Å^2) for $Li_{7-x}Sn_2$ (0.3 < x < 0.5). The Li atoms are refined isotropically (U_{eq} = U_{iso})

Atom	Site	x	y	z	U_{eq}
$Li_{6.67}Sn_2$					
Sn1	4*j*	0.34610(4)	0	0	0.0107(1)
Sn2	4*g*	0	0.18646(2)	1/2	0.0108(1)
Li1	8*q*	0.3116(9)	0.1554(5)	1/2	0.026(2)
Li2	8*p*	0.149(1)	0.1503(8)	0	0.042(3)
Li3	4*h*	0.145(1)	0	1/2	0.021(2)
Li4	4*i*	0	0.3233(8)	0	0.025(3)
Li5	2*c*	1/2	0	1/2	0.033(4)
Li6 [b]	2*a*	0	0	0	0.06(2)
$Li_{6.5}Sn_2$					
Sn1	4*j*	0.34806(7)	0	0	0.0120(2)
Sn2	4*g*	0	0.18884(5)	1/2	0.0112(2)
Li1	8*q*	0.311(1)	0.154(1)	1/2	0.033(4)
Li2	8*p*	0.143(2)	0.145(2)	0	0.062(6)
Li3	4*h*	0.146(2)	0	1/2	0.037 (6)
Li4	4*i*	0	0.321(1)	0	0.041(6)
Li5	2*c*	1/2	0	1/2	0.037(8)

[a] U_{eq} is defined as one third of the trace of the orthogonalized U_{ij} tensor. The anisotropic displacement factor exponent takes the form: $-2\pi^2[(ha^*)^2U_{11} + \ldots + hka^*b^*U_{12}]$. [b] The position is freely refined as *ca.* 1/3 occupied without a constraint on U_{iso}.

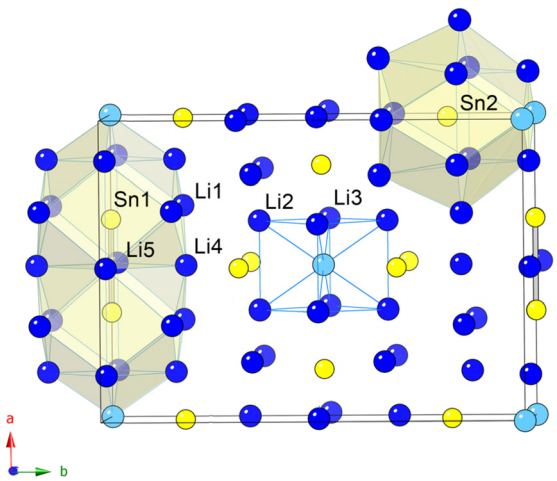

Fig. 3 Structure of $Li_{7-x}Sn_2$ (0.3 < x < 0.5). Blue represents Li atoms, Sn atoms are drawn in yellow. Missing/partially occupied Li atom is shown in lighter blue with thin blue lines connecting its closest Li neighbors. The Li-polyhedra around the Sn_2 dumbbell and the Sn atoms are also emphasized.

solid evidence for statistically significant deviations from 100%, which indicates that "filling" of the 2*a* site in the structure by a Li atom may not be favorable.

Although the structure of $Li_{17}Sn_4$ is completely different, we note that it has similar issues concerning one of the Li atoms. When the structure of $Li_{17}Sn_4$ was refined from our own single-crystal X-ray diffraction data (Tables S5 and S10 in SI), there was a residual density of 2.8 e Å^{-3}, located at coordinates 0,0,0 and at a distance of approx. 2.5 Å from another Li atom (whose occupancy was checked and verified to be very close to 100%). Refining the residual density as fully occupied Li atom was possible, but resulted in unphysical U_{iso} parameter. In the final refinement cycles, U_{iso} for the said Li position, Li13, had to be constrained (N. B. in their combined single-crystal X-ray and powder neutron diffraction work on $Li_{17}Sn_4$, Guloy *et al.* also used constraints on this very same Li site).[10] By comparison, when the structures of $Li_{13}Sn_5$ and Li_7Sn_3 were refined, there were no Li–Li contacts shorter than 2.75–2.8 Å (Tables S8 and S9 in SI) and we were able to even refine most of the Li atoms with anisotropic displacement parameters.

We also note that there does not seem to be a clear dependence on how the structures are refined with regards to the lithium content in the samples with nominal compositions of 6.7 : 2, 6.50 : 2, 6.25 : 2, and 6.00 : 2. In all of these cases, the residual density located at coordinates 0,0,0 was less than 0.5–0.6 e Å^{-3}. The highest residual peaks were of about 1–1.5 e Å^{-3}, always less than 1 Å away from other (always different) atoms, whose occupation factors show no evidence for statistically significant deviations from 100%. It is possible though, that some small disorder due to Li mobility in the structure is present, but it remains elusive from the structural data we have at hand. Taken together, all of the above is suggestive of the actual structure being with some Li disorder and with variable composition $Li_{7-x}Sn_2$ (0.3 < x < 0.5), not the Li_7Sn_2 as previously thought.[9]

Having alluded to some subtle structural features already, let us now look at the whole atomic arrangement in more details. As mentioned earlier, the ideal, disorder-free structure is known as isotypic with Li_7Ge_2 (space group *Cmmm*, no. 65; Z = 4; Pearson symbol *oS*36).[30] Within the asymmetric unit, there are eight crystallographically unique atomic positions (Table 2, Fig. 3): two tin atoms located at the 4*j* and 4*g* sites and six lithium atoms at the 2*a*, 2*c*, 4*h*, 4*i*, 8*p*, and 8*q* sites. With Li6 at 2*a* being either partially occupied or missing altogether, the formulation $Li_{7-x}Sn_2$ (0.3 < x < 0.5) would be a more accurate representation. This is in line with the reassessment of the Li_7Ge_2 structure in 1988 as $Li_{6.5}Ge_2 \equiv Li_{13}Ge_4$, although the exact structural details are not readily available in the literature.[15] Our own single-crystal data, provided in Table S2 in the SI section, confirm that the 2*a* site in the structure is empty and unlikely to host a Li atom due to the unphysically short distances to neighboring atoms, hence the composition $Li_{13}Ge_4$.

The structure of $Li_{7-x}Sn_2$ features key structural motifs previously described by Frank *et al.* (1975).[9] Unlike the more lithium-rich phases, such as $Li_{17}Sn_4$ [10,11] and Li_5Sn,[12] where all tin atoms are isolated, $Li_{7-x}Sn_2$ contains both isolated tin atoms and tin dumbbells (Fig. 3). The refined bond lengths within the Sn1–Sn1 dumbbells vary between 2.9838(13) Å ($Li_{6.5}Sn_2$) and 3.0131(7) Å ($Li_{6.7}Sn_2$). This is additional experimental evidence lending support to the formulation $Li_{7-x}Sn_2$: since Sn–Sn distances vary a lot more than 3–4σ, one may reason that slightly varied Li concentration is a contributing factor. Furthermore, one should also notice that although the refinements of Li occupancies are not conclusive, the refinements of Sn–Sn distances show the structure where Sn is for-

mally more reduced ($Li_{6.67}Sn_2$) to exhibit longer Sn1–Sn1 distance. Such variations of Ge–Ge distances are not observed in the 3 independent refinements of $Li_{7-x}Ge_2$ (bond lengths in the interval 2.607(1) to 2.615(2) Å, Table S7). This indicates that the germanide is more akin to a line phase $Li_{6.5}Ge_2 \equiv Li_{13}Ge_4$, confirming the earlier suggested reformulation of Li_7Ge_2 as $Li_{13}Ge_4$.[16]

Along these lines, considering other Li–Sn phases with high Li contents and structures featuring smaller molecular-like fragment is also instructive. For example, Sn–Sn bond lengths within the dumbbells in $Li_{5-x}Sn_{2+x}$ ($0 < x < 0.1$) are approx. 2.86 Å and vary from sample to sample.[7] For $Li_{13}Sn_5$, variations of Sn–Sn distances are not observed (2.865(1) and 2.8653(6) Å); Sn–Sn distances within the bent [Sn_3] moiety in Li_7Sn_3 are also nearly invariant of the sample (3–5σ deviations with an average value of approx. 2.94 Å [Table S9]). With the Sn atom formally being in its most reduced state in $Li_{6.67}Sn_2$, it is reasonable to expect the Sn–Sn bonding to be stretched farthest. As discussed in the next chapter, based on simple partitioning of the valence electrons following the Zintl–Klemm concept[31,32] and based on the electronic structure calculations, it is reasonable to approximate the $[Sn–Sn]^{6-}$ fragment in $Li_{7-x}Sn_2$ as isosteric with the I_2 molecule (*i.e.*, single covalent bond). The less reduced Sn atoms in $Li_{5-x}Sn_{2+x}$ ($0 < x < 0.1$) and $Li_{13}Sn_5$ ought to share more valence electrons, meaning that the $[Sn–Sn]^{4.5-}$ fragments in those will be more like the super-oxo $[O_2]^-$ species (*i.e.*, intermediate between single and double covalent bond). By analogy, the bent $[Sn_3]^{7-}$ in Li_7Sn_3, the least reduced stannide from the list, will have to be considered as isosteric with the allyl anion, $[H_2C–CH{=}CH_2]^-$.

The isolated tin atoms and the tin dumbbells are well separated, with the shortest contacts between Sn1 and Sn2 on the order of 4.9 Å; Sn2 and Sn2 are more than 4.7 Å apart. Sn atoms have 12 nearest Li atoms neighbors (not counting the partially occupied Li) (Fig. 3). The dumbbells and isolated tin atoms are distinctly arranged in a layered manner, with each type located in separate *ab*-planes. The Sn–Li distances range from 2.79 to 3.23 Å, and Li–Li distances also vary significantly, ranging from as short as 2.5 Å to over 3.5 Å (SI, Table S6).

Electronic structure and chemical bonding

First, let us try to rationalize the chemical bonding from the standpoint of the Zintl–Klemm concept.[31,32] Following the discussion from the preceding section, the valence electrons in $Li_7Sn_2 \equiv Li_{14}Sn_4$ and $Li_{13}Sn_4$ can be partitioned in a manner consistent with the tin dumbbells being $[Sn–Sn]^{6-}$ *i.e.*, single-bonded and isosteric with the I_2 molecule. We can then express their formulae in the following way: $Li_{14}Sn_4 = (Li^+)_{14}[Sn_2]^{6-}(Sn^{4-})_2$ and $Li_{13}Sn_4 = (Li^+)_{13}[Sn_2]^{6-}(Sn^{4-})_2(h^+)$, where h^+ denotes an electron–hole. Similarly, the formula of Li_7Sn_3 can be written as $(Li^+)_7[Sn_3]^{7-}$ (recognizing the analogy with the allyl anion) or as $(Li^+)_7[Sn_3]^{8-}(h^+)$ (treating both Sn–Sn bonds as 2-center 2-electron interactions). $Li_{13}Sn_5$ with the intermediate Sn–Sn bonding can be expressed as $(Li^+)_{13}([Sn_2]^{5-})_2(Sn^{4-})^-(h^+)$ or $(Li^+)_{13}([Sn_2]^{4.5-})_2(Sn^{4-})$ when further "oxidation" of the dumbbell is allowed. Clearly, simple bonding theories do not capture the details of the chemical bonding in these compounds, as the only formula that can be readily charge-balanced is that of $Li_{14}Sn_4$.

Electronic structure calculations were carried out for two structural models: $Li_7Sn_2 \equiv Li_{14}Sn_4$, where the Li position at Wyckoff site 2*a* is completely filled, and $Li_{6.5}Sn_2 \equiv Li_{13}Sn_4$, where the said position is empty. The total and projected densities of states for $Li_{14}Sn_4$ and $Li_{13}Sn_4$ are shown in Fig. 4 and 5. Electronic structure calculations for $Li_{13}Sn_5$ and Li_7Sn_3 are also done and are shown as figures in the SI.

The difficulties with balancing charges are reflected by the plots of the total and projected densities of states. From the calculated position of the Fermi level (E_F), it is apparent that both computed model structures do not represent valence-precise compounds as there are no noticeable (pseudo)gaps at E_F. Notice that the $Li_{14}Sn_4$ and $Li_{13}Sn_4$ differ by just one electron and the inclusion of the "extra" lithium atom in the calculation has a very small effect on the overall DOS. Lack of gaps in the electronic band structures is also seen in the cases of the other lithium stannides, Li_7Sn_3 and $Li_{13}Sn_5$ that were re-

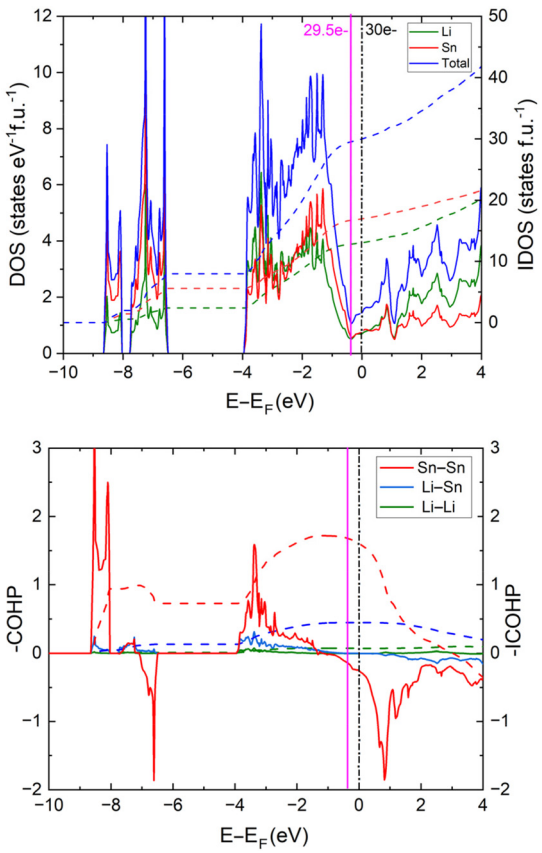

Fig. 4 Calculated total electronic density of states (DOS) and partial densities of states (pDOS) for Li_7Sn_2 (top). Crystal orbital Hamilton population (COHP) curves for averaged Sn–Sn, Sn–Li, and Li–Li interactions in $Li_{14}Sn_4$ (bottom). The dashed lines correspond to the Integrated Density of State (IDOS). The vertical magenta line to the left of the Fermi level shows the location of a pseudo-gap corresponding to *ca.* 29.5 valence electrons per unit cell ($Li_{\sim 6.75}Sn_2$).

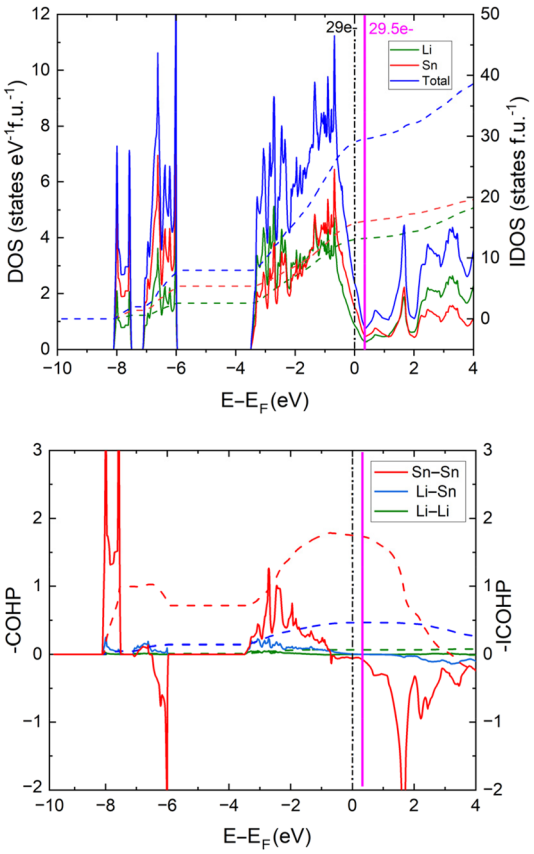

Fig. 5 Calculated total electronic density of states (DOS) and partial densities of states (pDOS) for $Li_{13}Sn_4$ (top). Crystal orbital Hamilton population (COHP) curves for averaged Sn–Sn, Sn–Li, and Li–Li interactions in $Li_{13}Sn_4$ (bottom). The dashed lines correspond to the Integrated Density of State (IDOS). The vertical magenta line to the right of the Fermi level shows the location of a pseudo-gap corresponding to *ca.* 29.5 valence electrons per unit cell ($Li_{\sim 13.5}Sn_4$).

evaluated in this work (SI Fig. S1–S4). Thus, all stannides discussed above will be expected to be compounds with metallic properties.

However, very close to the Fermi level, pseudogaps are apparent. Notably, within the rigid band approximation, the Fermi level can be shifted to the local minimum when the electron count is set at *ca.* 29.5 e. This value is intermediate between $Li_{13}Sn_4$ (29 e) and $Li_{14}Sn_4$ (30 e). This observation is an indirect evidence of support of the proposed off-stoichiometry of the $Li_{7-x}Sn_2$ phase as neither end member is expected to have greater electronic stability than the phase with partial occupancy of the Li 2*a* site. As discussed earlier, the lack of refineable electron density at that position does not rule out small possible disordering elsewhere in the structure that would lead to an upended Li content in alignment with this electronic structure analysis. Consequently, we argue that both experimental and computation evidence support the re-assessment of Li_7Sn_2 as $Li_{7-x}Sn_2$ where x will always be less than 0.5.

The corresponding Crystal Orbital Hamilton Population (COHP) curves for selected interactions in $Li_{14}Sn_4$ and $Li_{13}Sn_4$ are very much alike. The strongest bonds, based on the integrated COHP per bond, are the Sn–Sn bonds. However, these bonds are not fully optimized at the Fermi level due to the presence of some antibonding states. In fact, the Sn–Sn COHP at Fermi level in $Li_{14}Sn_4$ has more pronounced antibonding character compared to $Li_{13}Sn_4$, where the COHP is almost non-bonding. Since the Sn–Sn interactions in $Li_{13}Sn_4$ display a lower occupation of antibonding states, one would expect stronger Sn–Sn bonds, which is supported by the experimentally observed shorter Sn–Sn bond lengths in $Li_{6.5}Sn_2 \equiv Li_{13}Sn_4$ as compared to those in $Li_{6.67}Sn_2 \equiv Li_{13.3}Sn_4$.

In contrast, the Li–Sn and Li–Li interactions are effectively optimized at E_F. It appears that as the difference of a single Li atom alters the coordination environments and orbital overlap significantly enough to strengthen the Sn–Sn interactions and provide the "drive" for the phase to move away for the ideal "7–2" composition.

To compare relative stabilities of binary Li stannides in the vicinity of the $Li_{7-x}Sn_2$ composition, we first computed total energies of Li_7Sn_2 and $Li_{13}Sn_5$. The latter composition has been reported to be in equilibrium with Li_7Sn_2 at the Li/Sn ratios between 2.6 and 3.5.[33] After that, we evaluated the total energies of two ordered $Li_{7-x}Sn_2$ models: $Li_{13}Sn_4$ and $Li_{27}Sn_8$. Comparison of the obtained values suggests that $Li_{13}Sn_4$ is about 3.4 meV per atom less stable, while $Li_{27}Sn_8$ is 0.8 meV per atom more stable that the corresponding mixtures of Li_7Sn_2 and $Li_{13}Sn_5$. In other words, $Li_{27}Sn_8$ is predicted to be on the convex hull in the Li–Sn system. Of course, the limited accuracy of the PBE calculations for estimation of the decomposition enthalpies should not be ignored,[34] but in general, our calculations support the experimental observation that $Li_{7-x}Sn_2$ can be stabilized for a range of values $x > 0$. Furthermore, the composition of the idealized $Li_{27}Sn_8 \equiv Li_{13.5}Sn_4$ corresponds to 29.5 valence electrons per formula unit. The predicted thermodynamic stability of this phase is in line with the optimized chemical bonding at that electron count suggested by the LMTO calculations.

Conclusions

Li_7Sn_2 has been known for nearly five decades and is now shown to exhibit notable lithium site defects. The present study reveals that one specific Li site—namely, the 2*a* Wyckoff position is either partially or completely unoccupied. This observation leads to a revised composition of $Li_{7-x}Sn_2$, with x ranging between 0.3 and 0.5. Structural analysis across multiple samples shows no clear correlation between nominal Li : Sn ratio and occupational disorder, however Sn–Sn interactions do indicate structural response scaling with Li content. Comparative analysis with related stannides (Li_7Sn_3 and $Li_{13}Sn_5$) emphasizes consistent trends between bond lengths and bonding strength.

$Li_{7-x}Sn_2$, as well as other Li-rich germanides and stannides show metallic characteristics, making it difficult for the valence rules and the Zintl concept to sufficiently account for

the observed vacancies at Li sites in these compounds. These limitations underscore the broader challenges in accurately resolving Li positions and occupancies through crystallography and structural analysis.

To address these challenges and gain deeper insights into the site-specific behavior of alkali elements in tetrelides systems, investigation of analogous Na-containing compounds is in order. Given sodium's higher electron counts and expected chemical similarity to Li, Na-based systems may offer improved structural resolution and contribute to a more comprehensive understanding of alkali–tetrel interactions. Furthermore, these studies will also provide valuable knowledge applicable to the development of Na-ion battery technologies.

Author contributions

Salina Rahman: conceptualization, investigation, methodology, formal analysis, visualization, writing – original draft. Kowsik Ghosh: conceptualization, investigation, methodology, formal analysis, visualization, writing – original draft. Alexander Ovchinnikov: electronic structure calculations, formal analysis, chemical bonding analysis, writing – review & editing. Anirudh Nandakumar: investigation, formal analysis, writing – review & editing. Candace K. Chan: formal analysis, project administration, writing – review & editing. Svilen Bobev: conceptualization, supervision, project administration, writing – review & editing.

Conflicts of interest

There are no conflicts to declare.

Data availability

The data supporting this article have been included as part of the SI.

Tables with additional crystallographic data for all refined structures; DOS and COHP plots for $Li_{13}Sn_5$ and Li_7Sn_3. See DOI: https://doi.org/10.1039/d5dt01022e

CCDC 2444618–2444627, 2444630, 2444633 and 2444635 contain the supplementary crystallographic data for this paper.[35a–m]

Acknowledgements

This work was supported by the National Science Foundation through collaborative grants DMR-2004579 and DMR-2418368 (UD) and DMR-2004514 and DMR-2418367 (ASU). We acknowledge the use of facilities within the Eyring Materials Center at Arizona State University and assistance with PXRD measurements from R. Zhang, supported in part by NNCI-ECCS-1542160. NSF Major Research Instrumentation Award DMR-2217231: "MRI: Acquisition of a Dual Transmission X-ray Diffractometer (DTXRD) for Studying the Local and Bulk Structure of Soft and Hard Materials under *In situ* and Operando Conditions" is acknowledged for acquisition of the STOE Stadi P X-ray diffractometer.

References

1 C.-M. Park, J.-H. Kim, H. Kim and H.-J. Sohn, Li-alloy based anode materials for Li secondary batteries, *Chem. Soc. Rev.*, 2010, **39**, 3115–3141.
2 C.-Y. Chou, H. Kim and G. S. Hwang, A comparative first-principles study of the structure, energetics, and properties of Li–*M* (*M* = Si, Ge, Sn) alloys, *J. Phys. Chem. C*, 2011, **115**, 20018–20026.
3 D. Hansen and L. Chang, Crystal structure of Li_2Sn_5, *Struct. Sci.*, 1969, **25**, 2392–2395.
4 W. Müller and H. Schäfer, Die kristallstruktur der phase LiSn: the crystal structure of LiSn, *Z. Naturforsch., B*, 1973, **28**, 246–248.
5 W. Müller, Darstellung und Struktur der Phase Li_7Sn_3, *Z. Naturforsch., B*, 1974, **29**, 304–307.
6 U. Frank, W. Müller and H. Schäfer, Die Struktur der Phase Li_5Sn_2, *Z. Naturforsch., B*, 1975, **30**, 1–5.
7 K. Ghosh, S. Rahman, A. Ovchinnikov and S. Bobev, Applicability of the Zintl Concept to Understanding the Crystal Chemistry of Lithium-Rich Germanides and Stannides, *Inorg. Chem.*, 2024, **63**, 20173–20185.
8 U. Frank and W. Müller, Darstellung und Struktur der Phase $Li_{13}Sn_5$ und die Strukturelle Verwandtschaft der Phasen in den Systemen Li–Sn und Li–Pb, *Z. Naturforsch., B*, 1975, **30**, 316–322.
9 U. Frank, W. Müller and H. Schäfer, Die Kristallstruktur der Phase Li_7Sn_2, *Z. Naturforsch., B*, 1975, **30**, 6–9.
10 C. Lupu, J.-G. Mao, J. W. Rabalais, A. M. Guloy and J. W. Richardson, X-ray and neutron diffraction studies on "$Li_{4.4}Sn$", *Inorg. Chem.*, 2003, **42**, 3765–3771.
11 G. Goward, N. Taylor, D. Souza and L. Nazar, The true crystal structure of $Li_{17}M_4$ (*M* = Ge, Sn, Pb) – revised from $Li_{22}M_5$, *J. Alloys Compd.*, 2001, **329**, 82–91.
12 R. U. Stelzer, Y. Ikeda, P. Srinivasan, T. S. Lehmann, B. Grabowski and R. Niewa, Li_5Sn, the most lithium-rich binary stannide: a combined experimental and computational study, *J. Am. Chem. Soc.*, 2022, **144**, 7096–7110.
13 J. Sangster and C. W. Bale, The Li-Sn (lithium-tin) system, *J. Phase Equilib.*, 1998, **19**, 70–75.
14 M. Mayo, J. P. Darby, M. L. Evans, J. R. Nelson and A. J. Morris, Correction to structure prediction of Li–Sn and Li–Sb intermetallics for lithium-ion batteries anodes, *Chem. Mater.*, 2018, **30**, 5516–5517.
15 V. Hopf, W. Müller and H. Schäfer, Die Struktur der Phase Li_7Ge_2, *Z. Naturforsch., B*, 1972, **26**, 1157–1160.
16 R. Nesper, *Synthese, Struktur und Eigenschaften von Verbindungen im Grenzbereich zwischen Zintl-Phasen und Metallen: experimentelle und quantenmechanischen Beiträge*

zum Verständnis der chemischen Bindung im Grenzbereich zwischen Halbleitern und Metallen und topologische Konzepte zur Struktursytematik. *Habilitation Thesis*, Universität Stuttgart, 1988.

17 U. Frank, W. Müller and H. Schäfer, Zur Kenntnis der Phase $Li_{13}Si_4$, *Z. Naturforsch., B*, 1975, **30**, 10–13.

18 M. Zeilinger and T. F. Fässler, Revision of the $Li_{13}Si_4$ structure, *Acta Crystallogr., Sect. E:Crystallogr. Commun.*, 2013, **69**, i81–i82.

19 A. J. Morris, C. P. Grey and C. J. Packard, Thermodynamically stable lithium silicides and germanides from density functional theory calculations, *Phys. Rev. B:Condens. Matter Mater. Phys.*, 2014, **90**, 054111.

20 O. V. Dolomanov, L. J. Bourhis, R. J. Gildea, J. A. K. Howard and H. Puschmann, OLEX2: a complete structure solution, refinement and analysis program, *J. Appl. Crystallogr.*, 2009, **42**, 339–341.

21 G. M. Sheldrick, Crystal structure refinement with SHELXL, *Acta Crystallogr., Sect. C:Struct. Chem.*, 2015, **71**, 3–8.

22 G. M. Sheldrick, SHELXT – Integrated space-group and crystal-structure determination, *Acta Crystallogr., Sect. A: Found. Adv.*, 2015, **71**, 3–8.

23 L. Gelato and E. Parthé, STRUCTURE TIDY – a computer program to standardize crystal structure data, *J. Appl. Crystallogr.*, 1987, **20**, 139–143.

24 O. K. Andersen and O. Jepsen, Explicit, first-principles tight-binding theory, *Phys. Rev. Lett.*, 1984, **53**, 2571.

25 U. von Barth and L. Hedin, A local exchange-correlation potential for the spin polarized case. i, *J. Phys. C Suppl.*, 1972, **5**, 1629.

26 S. Steinberg and R. Dronskowski, The crystal orbital Hamilton population (COHP) method as a tool to visualize and analyze chemical bonding in intermetallic compounds, *Crystals*, 2018, **8**, 225.

27 P. Giannozzi, O. Andreussi, T. Brumme, O. Bunau, M. Buongiorno Nardelli, M. Calandra, R. Car, C. Cavazzoni, D. Ceresoli, M. Cococcioni, N. Colonna, I. Carnimeo, A. Dal Corso, S. de Gironcoli, P. Delugas, R. A. DiStasio Jr, A. Ferretti, A. Floris, G. Fratesi, G. Fugallo, R. Gebauer, U. Gerstmann, F. Giustino, T. Gorni, J. Jia, M. Kawamura, H.-Y. Ko, A. Kokalj, E. Küçükbenli, M. Lazzeri, M. Marsili, N. Marzari, F. Mauri, N. L. Nguyen, H.-V. Nguyen, A. Otero-de-la-Roza, L. Paulatto, S. Poncé, D. Rocca, R. Sabatini, B. Santra, M. Schlipf, A. P. Seitsonen, A. Smogunov, I. Timrov, T. Thonhauser, P. Umari, N. Vast, X. Wu and S. Baroni, *J. Phys.: Condens. Matter*, 2017, **29**, 465901.

28 J. P. Perdew, K. Burke and M. Ernzerhof, Generalized Gradient Approximation Made Simple, *Phys. Rev. Lett.*, 1996, **77**, 3865.

29 D. Vanderbilt, Soft self-consistent pseudopotentials in a generalized eigenvalue formalism, *Phys. Rev. B:Condens. Matter Mater. Phys.*, 1990, **41**, 7892.

30 P. Villars and L. D. Calvert, *Pearson's handbook of crystallographic data for intermetallic phases*, American Society for Metals, Metals Park, 1986.

31 S. M. Kauzlarich, *Chemistry, structure, and bonding of Zintl phases and ions*, VCH, New York, 1998.

32 R. Nesper, The Zintl–Klemm concept – a historical survey, *Z. Anorg. Allg. Chem.*, 2014, **640**, 2639–2648.

33 S. Fürtauer and H. Fladorfer, The Cu-Li-Sn phase diagram: Isothermal sections, *J. Alloys. Compd.*, 2016, **682**, 713.

34 G. Hautier, S. P. Ong, A. Jain, C. J. Moore and G. Ceder, Accuracy of density functional theory in predicting formation energies of ternary oxides from binary oxides and its implication on phase stability, *Phys. Rev. B: Condens. Matter Mater. Phys.*, 2012, **85**, 155208.

35 (*a*) S. Rahman, K. Ghosh, A. Ovchinnikov, A. Nandakumar, C. K. Chan and S. Bobev, CCDC 2444618: Experimental Crystal Structure Determination, 2025, DOI: **10.5517/ccdc.csd.cc2n1tn6**; (*b*) S. Rahman, K. Ghosh, A. Ovchinnikov, A. Nandakumar, C. K. Chan and S. Bobev, CCDC 2444619: Experimental Crystal Structure Determination, 2025, DOI: **10.5517/ccdc.csd.cc2n1tp7**; (*c*) S. Rahman, K. Ghosh, A. Ovchinnikov, A. Nandakumar, C. K. Chan and S. Bobev, CCDC 2444620: Experimental Crystal Structure Determination, 2025, DOI: **10.5517/ccdc.csd.cc2n1tq8**; (*d*) S. Rahman, K. Ghosh, A. Ovchinnikov, A. Nandakumar, C. K. Chan and S. Bobev, CCDC 2444621: Experimental Crystal Structure Determination, 2025, DOI: **10.5517/ccdc.csd.cc2n1tr9**; (*e*) S. Rahman, K. Ghosh, A. Ovchinnikov, A. Nandakumar, C. K. Chan and S. Bobev, CCDC 2444622: Experimental Crystal Structure Determination, 2025, DOI: **10.5517/ccdc.csd.cc2n1tsb**; (*f*) S. Rahman, K. Ghosh, A. Ovchinnikov, A. Nandakumar, C. K. Chan and S. Bobev, CCDC 2444623: Experimental Crystal Structure Determination, 2025, DOI: **10.5517/ccdc.csd.cc2n1ttc**; (*g*) S. Rahman, K. Ghosh, A. Ovchinnikov, A. Nandakumar, C. K. Chan and S. Bobev, CCDC 2444624: Experimental Crystal Structure Determination, 2025, DOI: **10.5517/ccdc.csd.cc2n1tvd**; (*h*) S. Rahman, K. Ghosh, A. Ovchinnikov, A. Nandakumar, C. K. Chan and S. Bobev, CCDC 2444625: Experimental Crystal Structure Determination, 2025, DOI: **10.5517/ccdc.csd.cc2n1twf**; (*i*) S. Rahman, K. Ghosh, A. Ovchinnikov, A. Nandakumar, C. K. Chan and S. Bobev, CCDC 2444626: Experimental Crystal Structure Determination, 2025, DOI: **10.5517/ccdc.csd.cc2n1txg**; (*j*) S. Rahman, K. Ghosh, A. Ovchinnikov, A. Nandakumar, C. K. Chan and S. Bobev, CCDC 2444627: Experimental Crystal Structure Determination, 2025, DOI: **10.5517/ccdc.csd.cc2n1tyh**; (*k*) S. Rahman, K. Ghosh, A. Ovchinnikov, A. Nandakumar, C. K. Chan and S. Bobev, CCDC 2444630: Experimental Crystal Structure Determination, 2025, DOI: **10.5517/ccdc.csd.cc2n1v1m**; (*l*) S. Rahman, K. Ghosh, A. Ovchinnikov, A. Nandakumar, C. K. Chan and S. Bobev, CCDC 2444633: Experimental Crystal Structure Determination, 2025, DOI: **10.5517/ccdc.csd.cc2n1v4q**; (*m*) S. Rahman, K. Ghosh, A. Ovchinnikov, A. Nandakumar, C. K. Chan and S. Bobev, CCDC 2444635: Experimental Crystal Structure Determination, 2025, DOI: **10.5517/ccdc.csd.cc2n1v6s**.